Eur. Phys. J. D **20**, 375–388 (2002)
DOI: 10.1140/epjd/e2002-00160-9

THE EUROPEAN PHYSICAL JOURNAL D

Tautomery and H-bonding characteristics of 2-aminopurine: a combined experimental and theoretical study*

R. Ramaekers[1], L. Adamowicz[2], and G. Maes[1,a]

[1] Department of Chemistry, University of Leuven, Celestijnenlaan 200 F, 3001 Heverlee, Belgium
[2] Department of Chemistry, University of Arizona, Tucson, Arizona 85721, USA

Received 10 December 2001
Published online 13 September 2002

Abstract. An experimental and theoretical RHF, MP2 and DFT/6-31++G** study is described of the matrix FT-IR spectra of monomer 2-aminopurine and H-bonded complexes of 2-aminopurine with water. 2-aminopurine occurs in Ar predominantly as the amino–N9H tautomer, but small amounts of the amino–N7H tautomer are also present. An approximate K_T value for this tautomeric equilibrium is found to be 0.016 (RHF) and 0.015 (DFT) using the infrared intensity measurement. Four H-bonded complexes of the abundant amino–N9H form with water are detected in the experimental FT-IR spectrum by their characteristic predicted absorptions, *i.e.* the three closed complexes N3···H–O···H–N9, N1···H–O···H–NH, N3···H–O···H–NH and the open complex N7···H–OH. From the experimental results, the proton affinity of the N7 atom in 2-aminopurine can be estimated. The dependence of the H-bond strength on the H-bond linearity is demonstrated by a correlation between the N···H distance and the N···H–O angle in closed N···H–O···H–N complexes.

PACS. 87.14.Gg DNA, RNA – 87.15.Aa Theory and modeling; computer simulation – 87.15.By Structure and bonding

1 Introduction

2-aminopurine (2AP) is a purine derivate comparable to adenine and guanine, the only difference with adenine being the position of the amino group. It is a fluorescent adenine isomer which can be incorporated into DNA during replication without obstructing the base pairing, so that 2AP preserves the B-form DNA. These properties of 2AP have been used to study the structure and dynamics of DNA fragments by replacing adenine by the fluorescent isomer 2AP. 2-aminopurine is also a potential mutagen in bacteria, generating predominantly transition mutations as a consequence of different base pairing. Whereas adenine and 2-aminopurine normally pair with thymine, 2-aminopurine can also form a base pair with cytosine [1,2]. This implies that 2-aminopurine can produce AT⇌GC transitions in the next generation.

Literature data on the tautomeric properties of the ground state of 2-aminopurine are scarce. Sheina *et al.* [3] have compared the theoretically predicted IR spectra of 2AP with those of adenine. They have concluded that the change in the position of the amino group on the pyrimidine ring has no large influence on the IR spectrum, some changes of the stretching vibrations of the pyrimidine ring being observable only in the low frequency region. The N7H⇌N9H equilibrium in vacuum and in water has been studied theoretically by Broo *et al.* [4]. These authors have concluded that in vacuum (MP2/6-31G* level) the amino–N9H tautomer is favored over amino–N7H by 18.8 kJ mol^{-1}, whereas the imino–N1H–N9H form was found to be 127 kJ mol^{-1} less stable. This prediction has later been confirmed by the same research group, *i.e.* the amino–N9H tautomer is abundant and only a very small amount (<1%) of the amino–N7H form exists at room temperature [5]. The Onsager and polarized continuum models have been used in self-consistent reaction field calculations to describe the solvent-solute interaction [4]. In water solution, the amino–N7H form is slightly stabilized relative to the N9H tautomer, the energy difference being decreased to 11.2 kJ mol^{-1}. The same authors [4] have also investigated the geometry of the amino–N9H tautomer in more detail using the DFT(B3LYP) method with different basis sets. From this study, it has been concluded that the improvement of the basis set favors an increase of the planarity of the amino group.

Recently more attention has been paid to the excited states of 2AP, because of the high fluorescence capacity of this molecule [6–8]. The position of the amino group

* The experimental spectrum of monomer 2-aminopurine and tables of energy data, experimental and theoretical predicted spectral parameters are only available in electronic form at `http://www.edpsciences.org`

[a] e-mail: `guido.maes@chem.kuleuven.ac.be`

on the C2 atom of the purine molecule appears to have a strong effect on the excited-state potentials [9].

The H-bond characteristics of 2-aminopurine have not been studied into great detail. Most literature data focus on the geometry of the 2AP·C mispair in DNA. An NMR study of the conformation of this base pair has been performed by Fagan *et al.* [10]. They have found that this mispair is of the wobble type. A series of UV, fluorescence, and NMR studies to determine the structure of the 2AP·C mispair, described by Sowers *et al.* [11], has demonstrated that an equilibrium exist between the neutral wobble and the protonated Watson-Crick structures. A quantum-chemical characterization of the cytosine·2AP base pair has been performed by Sherer *et al.* [12]. These calculations have indicated that in aqueous solution the Watson-Crick form of the 2AP·C base pair, protonated at the N1 atom of 2AP, is preferred over the neutral wobble pair. Literature data on H-bonded complexes of 2AP with water are not available hitherto.

2 Methodology

2.1 Experimental method

The cryogenic and FT-IR (Bruker IFS-88) equipment used here have been described in detail in earlier papers [13–15]. The solid compound 2-aminopurine was evaporated at 433 K in a home-made mini-furnace positioned close to the cold CsI window (15 K) in the cryostat. Water-doped argon matrices with different H_2O/Ar ratio were deposited for the study of the H-bonded complexes. Fairly high water-to-base ratios were used to ensure an excess amount of 1:1 H-bonded complexes 2AP/water. Former studies of H-bonded complexes have demonstrated that such ratios ensure excess amounts of the 1:1 complex to be formed without disturbing effects of higher-stoichiometry complexes [13].

Twice-distilled water was used for the experiments with water-doped matrices. The H_2O/Ar ratios were varied between 1/300 to 1/800.

Additional IR spectra were recorded for 2AP in a D_2O-doped Ar matrix.

2.2 Theoretical method

Molecular properties such as geometries, energies and vibrational frequencies of the different tautomers and H-bonded complexes were calculated using both the density functional theory (DFT) and the RHF method. The DFT method, with Becke's non-local three parameter exchange functional [16] and the gradient-corrected functional of Lee, Yang and Parr (B3LYP functional) [17], has been demonstrated in former studies to produce quite accurate results for isolated molecules modeling nucleic acid bases [18–22]. The standard 6-31++G** basis set was used in all these calculations. For a better description of the long-range interaction of H-bondings it is essential to employ sets of orbitals that possess sufficient diffuseness and angular flexibility. Therefore, an extension of the basis set with diffuse functions (++) is necessary.

The structure optimizations of the different forms at the RHF level was followed by single-point MP2 calculations with the frozen core electron option. This was necessary to account for electron correlation. The MP2 energy obtained for the RHF optimized molecular structures will be further denoted as MP2//RHF.

The H-bond interaction energy of each complex was computed as the difference between the energy of the complex and the energies of the monomer base and water. These results were corrected for the basis set superposition error (*BSSE*), by recalculating the monomer energies in the basis set of the hetero-dimers using the Boys-Bernardi counterpoise correction [23].

Finally, Potential Energy Distributions (PED) were calculated and the computed IR frequencies were scaled to account for various systematic errors in the theoretical approach, *i.e.* the use of a finite basis set, the neglect of the vibrational anharmonicity and the incomplete account for electron correlation. Either a single scaling factor was used (0.900 for RHF and 0.970 for DFT) or a set of different scaling factors was used (DFT), reflecting the difference in the anharmonicity of the different types of vibrational modes. The latter scaling procedure has been proposed by several authors in the recent past [24–26]. All calculations were performed with the Gaussian 94 and Gaussian 98 programs [27,28].

3 Results

3.1 Monomeric 2-aminopurine [29]

Combination of the amino⇌imino and the N1–H⇌N3–H⇌N7–H⇌N9–H prototropies allows 2-aminopurine to occur in 9 different tautomers, *i.e.* 4 amino forms and 5 imino forms. The orientation of the H atom on the imino N atom yields 5 extra isomers. This implies that 14 possible structures exist for 2-aminopurine. Figure 1 presents the optimal geometries of the four amino forms and five of the imino forms of 2-aminopurine.

According to the RHF, MP2//RHF and the DFT methodology with the 6-31++G** basis set, the amino–N9H form is the most stable tautomer, while the amino–N7H form is about 18 kJ mol^{-1} less stable (MP2 level). All the imino forms are at least 100 kJ mol^{-1} higher in energy. The MP2 and the DFT results agree very well in the prediction of the stability order of the 2AP tautomers.

From a detailed analysis of the experimental matrix FT-IR spectrum of 2AP, a value can be estimated for the equilibrium constant of the tautomerization process between the amino–N9H and the amino–N7H tautomers. The mean experimental K_T(N7H/N9H) value is found to be 1.6×10^{-2} at the RHF level and 1.5×10^{-2} at the DFT level of theory. The theoretical K_T values calculated from the relative energy differences between the tautomers at the different theoretical levels are 1.2×10^{-3} (RHF), 7.9×10^{-3} (MP2) and 6.8×10^{-3} (DFT), respectively.

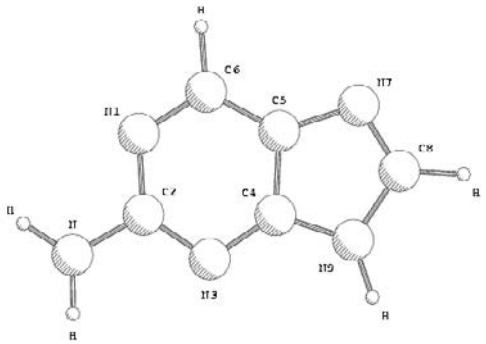

amino-N9H

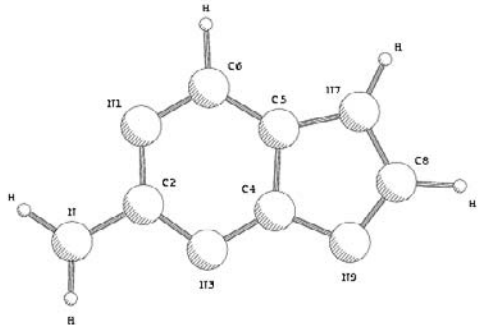

amino-N7H

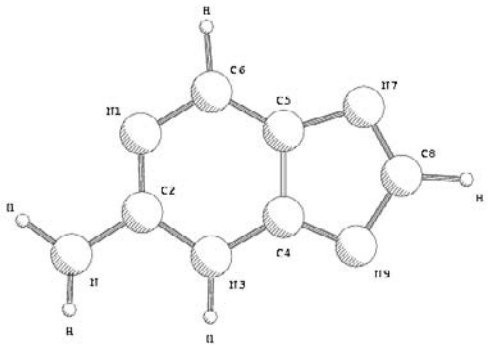

amino-N3H

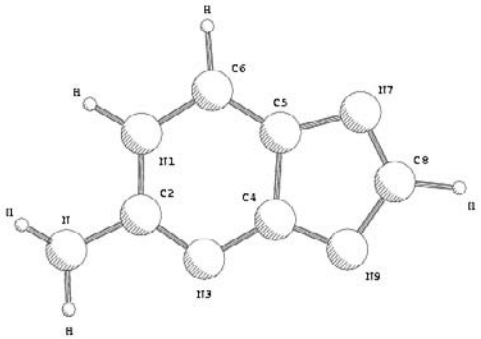

amino-N1H

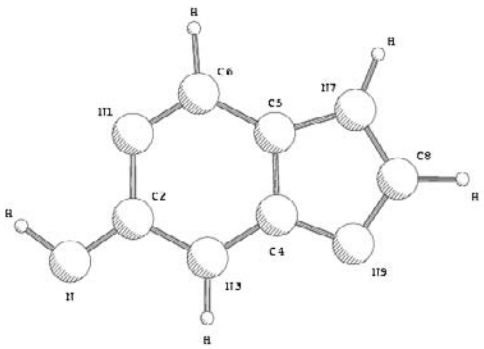

imino-N3H-N7H

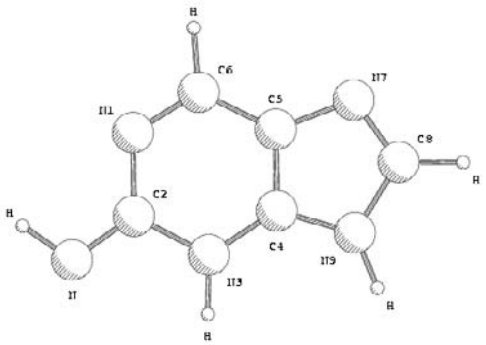

imino-N3H-N9H

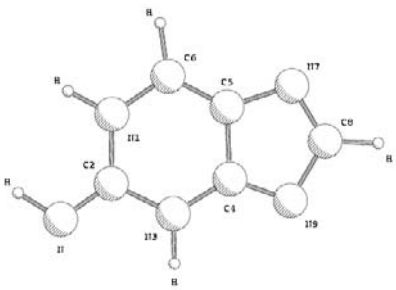

imino-N1H-N3H

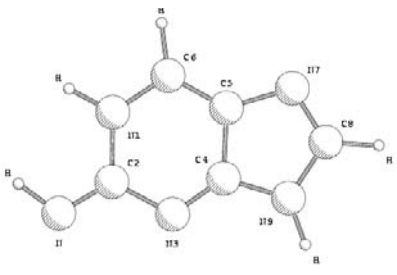

imino-N1H-N9H

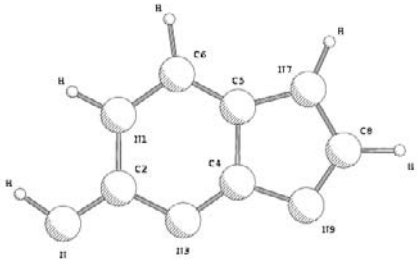

imino-N1H-N7H

Fig. 1. Optimal geometries of nine possible tautomers of 2-aminopurine.

Table 1. Total (a.u.) and relative energies (kJ mol^{-1}) of H-bonded complexes of the two most stable tautomers of 2-aminopurine with water.

	RHF[a]//RHF 6-31++G**	ΔE[b] (RHF//RHF)	μ (D) (RHF)	MP2[a]//RHF 6-31++G**	ΔE[b] (MP2//RHF)	DFT[c]//DFT 6-31++G**	ΔE[b] (DFT//DFT)	μ (D) (DFT)
Amino–N9H								
N3···H–O···H–N9	−540.458879	**0.00**	3.22	−542.131957	**0.00**	−543.667298	**0.00**	3.18
N1···H–O···H–NH	−540.457040	**4.83**	3.13	−542.129104	**7.49**	−543.666399	**2.36**	3.27
N3···H–O···H–NH	−540.455682	**8.39**	3.31	−542.127722	**11.12**	−543.664786	**6.60**	3.27
N7···H–OH	−540.455499	**8.87**	2.66	−542.126589	**14.09**	−543.663060	**11.13**	4.33
Amino–N7H								
N3···H–O···HN–H	−540.449110	**25.65**	5.97	−542.123835	**21.32**	−543.660392	**18.13**	5.43
N1···H–O···H–NH	−540.447029	**31.11**	6.20	−542.121569	**27.27**	−543.658701	**22.57**	5.63
N7–H···OH_2	−540.448727	**26.65**	8.17	−542.122662	**24.40**	−543.657902	**24.67**	7.71
N9···H–OH	−540.447831	**29.01**	3.81	−542.121009	**28.74**	−543.657391	**26.01**	4.83

[a] *ZPE*-corrected RHF and MP2 energies; *ZPE* values scaled with the scaling factor 0.900 (RHF).
[b] Energy difference between the complexes.
[c] *ZPE*-corrected DFT energies; *ZPE* values scaled with the scaling factor 0.970 (DFT).

The detailed energetic data of the different tautomeric forms of 2AP and the detailed analysis of the vibrational spectrum are available from the corresponding author on request.

3.2 H-bonding properties of 2-aminopurine

The investigation of the H-bonding properties of 2AP is limited to the two most stable tautomers identified in the study of the tautomeric properties of 2AP [29], *i.e.* the amino–N9H and the amino–N7H forms.

The amino–N9H tautomer has three H-bond donor sites, *i.e.* the two amino N–H groups and N9–H, and three H-bond acceptor sites, *i.e.* N1, N3 and N7. The H-bonding sites of the amino–N7H tautomer are comparable to those of the amino–N9H form, *i.e.* three H-bond donor sites (two amino N–H groups and N7–H) and three H-bond acceptor sites (N1, N3 and N9). The vicinal position of the H-bond donor and acceptor sites allows the formation of closed complexes. Four different complexes with water are possible for both tautomers, three of these being closed H-bonded complexes with two H-bonds. For the amino–N9H tautomer the four complexes with water are N1···H–O···H–NH, N3···H–O···H–NH, N3···H–O···H–N9 and N7···H–OH. For the amino–N7H tautomer, the complexes are N1···H–O···H–NH, N3···H–O···H–NH, N9···H–OH and N7–H···OH_2.

The geometry optimizations for the eight complexes described above were performed on the RHF and DFT levels of theory. Table 1 lists the total and relative energies of all these structures at the RHF, MP2//RHF and DFT level with the 6-31++G** basis set. Figures 2 and 3 show the optimal geometries of the complexes for amino–N9H and amino–N7H, respectively.

The strength of the H-bonding in the different complexes was also calculated on the different levels of theory. Table 2 summarizes the H-bond interaction energies at three levels of accuracy, *i.e.* the differences between the energies of the complex and the monomers (=ΔE), with addition of the *ZPE* correction ($\Delta E + ZPE$), and with addition of the *ZPE* as well as the *BSSE* correction ($\Delta E + ZPE - BSSE$).

As expected, the most stable complex N3···H–O···H–N9 has the largest (*i.e.* strongest complex) interaction energy at all levels of theory. Closed H-bonded complexes are generally stronger (larger interaction energy and higher stability) than open complexes, because of the H-bond cooperativity effect [30].

MP2 interaction energies are mostly larger than DFT and RHF interaction energies. For some of the 2AP complexes, the *BSSE* correction reverses this order. This is the case for the complexes were the amino group is involved, *i.e.* N1···H–O···H–NH and N3···H–O···H–NH, for both tautomers.

Although the N1···H–O···H–NH and N3···H–O···H–NH complexes exist for both tautomers, the stability order of the two complexes is different.

In two open complexes, *i.e.* N7···H–OH of the amino–N9H tautomer and N9···H–OH of the amino–N7H tautomer, the water molecule is orientated such that a weak interaction might take place between the O atom of water and the C8–H group of 2AP. If this interaction takes place, the C8–H distance should elongate. However, the elongation of this bond predicted at the RHF level is negligibly small (about 0.0002 Å). Also at the DFT level, the C8–H bond is shortened for only about 0.0002 Å. This implies that both complexes are really "open" complexes.

From the above theoretical results it can be expected that only the four complexes of the amino–N9H tautomer will be present in the experimental matrix isolation spectra of 2AP with water. First of all, only about 1% of 2AP is present as the amino–N7H form [29]. Furthermore, the complexes of the amino–N7H form are at least 18 kJ mol^{-1} (DFT) less stable and the probability to find these in the experimental spectrum is therefore very small.

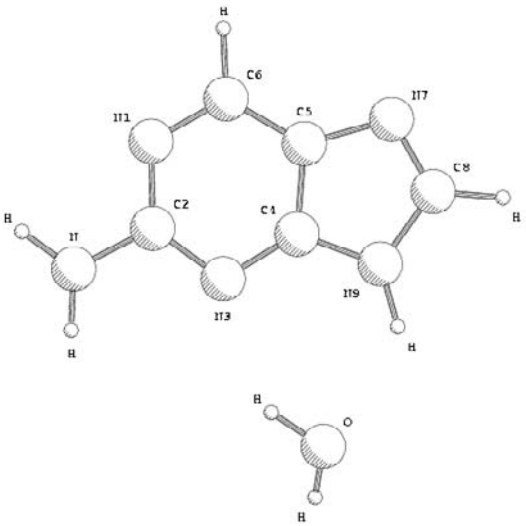

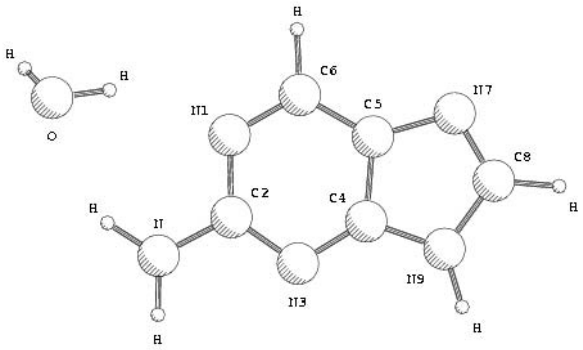

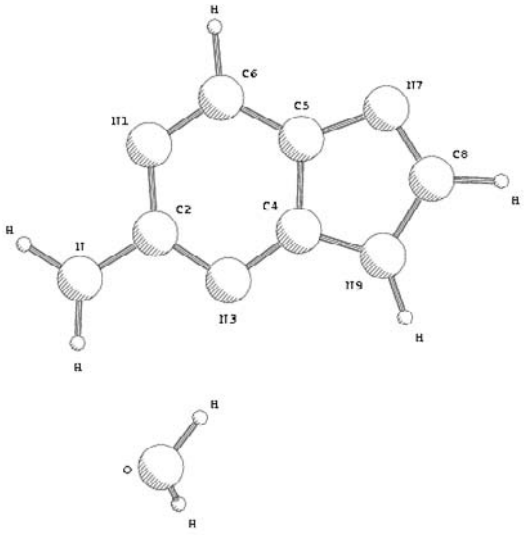

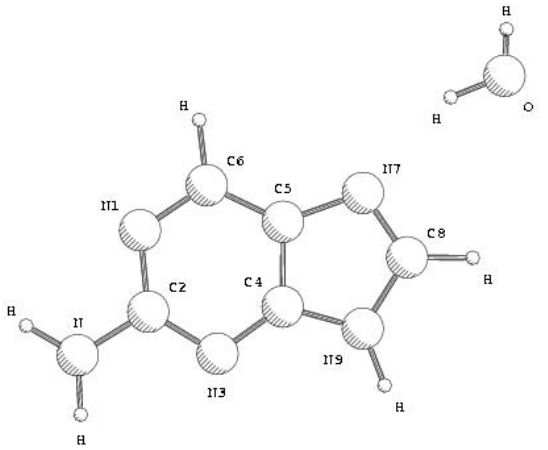

Fig. 2. Geometries of the four possible H-bonded complexes between (amino–N9H) 2-aminopurine and water.

The vibrational analysis of the experimental spectra was performed in terms of the four complexes of the amino–N9H tautomer. Tables 3–5 summarize the experimental and theoretical (only DFT) frequencies, frequency shifts, intensities and PEDs of the vibrational modes of the four complexes. Only vibrational modes directly involved in the H-bonding are listed. For the N7$\cdots$H–OH complex, only the vibrations of water are important, because the frequency shifts of the vibrations where the N7 atom is involved, *i.e.* ring stretching, ring bending and ring torsion vibrations are mostly rather small and these vibrations are usually less intense [35]. The different spectral regions will be analyzed separately. Figures 4–7 illustrate the different regions of the experimental complex spectra.

3.2.1 $\nu^{f}_{O\text{-}H}$-region

When either a single H-bond, B$\cdots$H–OH, or two H-bonds, B$\cdots$H–O(H)$\cdots$H–A, are formed with water, only one of the OH groups is involved in the H-bonding, while the

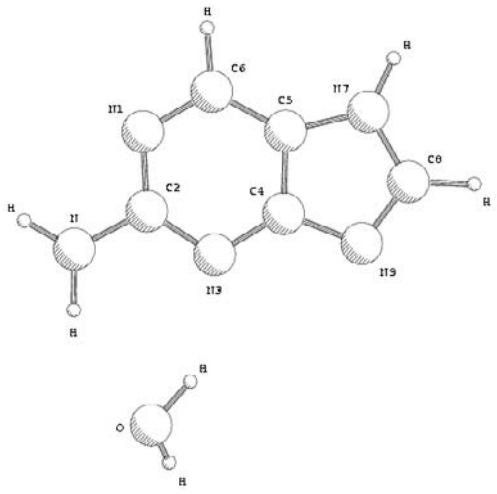

N3···H-O···H-NH

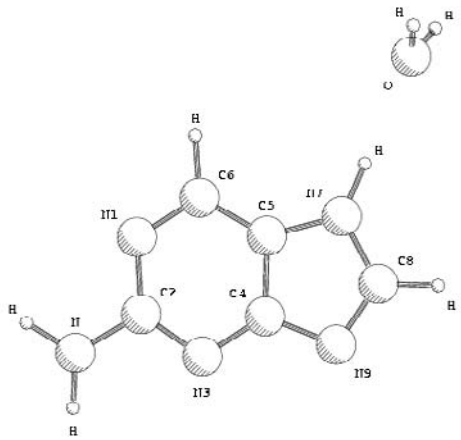

N7-H···OH_2

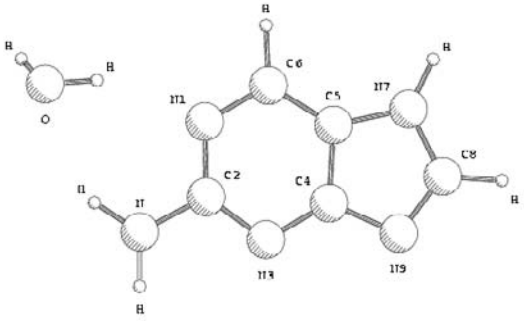

N1···H-O···H-NH

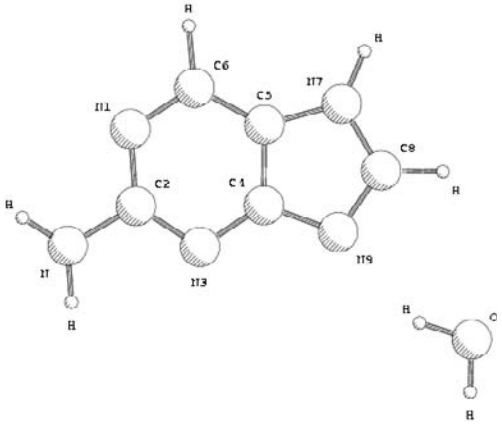

N9···H-OH

Fig. 3. Geometries of the four possible H-bonded complexes between (amino–N7H) 2-aminopurine and water.

other OH group remains free. We will distinguish between these groups by the vibrational symbolism $\nu^{\mathrm{f}}_{\mathrm{O\text{-}H}}$ (for free) and $\nu^{\mathrm{b}}_{\mathrm{O\text{-}H}}$ (for bonded).

It is not possible to make any distinction between the four complexes, N3$\cdots$H–O$\cdots$H–N9 (1), N1$\cdots$H–O$\cdots$H–NH (2), N3$\cdots$H–O$\cdots$H–NH (3) and N7$\cdots$H–OH (4), based on the $\nu^{\mathrm{f}}_{\mathrm{O\text{-}H}}$-region, because the predicted $\nu^{\mathrm{f}}_{\mathrm{O\text{-}H}}$ frequencies have all about the same shift (-39, -43, -44, -42 cm^{-1}, respectively) with respect to the theoretical monomer frequency of 3 735 cm^{-1}. However, complex formation is clearly manifested in the experimental spectrum. As a matter of fact, in the pure water spectrum there is no band at 3 700 cm^{-1}, while in the complex spectrum a band appears at 3 700 cm^{-1}. This band can be assigned to the free O–H stretching vibration of H_2O in the four different H-bonded complexes 2AP·H_2O.

3.2.2 $\nu^{\mathrm{b}}_{\mathrm{O\text{-}H}}$ and $\nu_{\mathrm{N\text{-}H}}$ region

Figure 4 illustrates the spectral region between 3 600 and 3 100 cm^{-1}. This region contains 2AP monomer absorptions, water absorptions, as well as complex absorptions. Spectrum A is scanned before annealing the matrix while spectrum B is scanned after annealing.

The frequency shifts of the bonded O–H frequencies of water in the four complexes differ much more than the shifts of the free O–H frequencies (Tab. 3). Three new, weak bands or shoulders appear at 3 407, 3 392 and 3 301 cm^{-1}, which can be assigned with good confidence to the $\nu^{\mathrm{b}}_{\mathrm{O\text{-}H}}$ mode of the N7$\cdots$H–OH (4), N3$\cdots$H–O$\cdots$H–N9 (1) and N1$\cdots$H–O$\cdots$H–NH (2) complexes, respectively. As a matter of fact, the corresponding shifts $\Delta\nu^{\mathrm{b}}_{\mathrm{O\text{-}H}}$ agree more or less with the predicted shifts of -204, -233

Table 2. Interaction energies (kJ mol^{-1}) of 2-aminopurine – water H-bonded complexes.

	RHF//RHF	MP2//RHF	DFT//DFT
Tautomer 1: Amino-N9H			
	N3$\cdots$H–O$\cdots$H–N9		
ΔE	−33.95	−47.61	−41.84
$\Delta E + \Delta ZPE$	−25.60	−39.26	−32.42
$\Delta E + \Delta ZPE - BSSE$	−23.10	−31.51	−29.18
	N1$\cdots$H–O$\cdots$H–NH		
ΔE	−28.54	−39.54	−38.89
$\Delta E + \Delta ZPE$	−20.77	−31.77	−30.06
$\Delta E + \Delta ZPE - BSSE$	−18.25	−24.08	−26.82
	N3$\cdots$H–O$\cdots$H–NH		
ΔE	−24.86	−35.80	−34.40
$\Delta E + \Delta ZPE$	−17.21	−28.14	−25.82
$\Delta E + \Delta ZPE - BSSE$	−14.70	−20.39	−22.58
	N7$\cdots$H–OH		
ΔE	−23.00	−31.44	−28.28
$\Delta E + \Delta ZPE$	−16.73	−25.17	−21.29
$\Delta E + \Delta ZPE - BSSE$	−14.86	−19.61	−19.08
Tautomer 2: Amino-N7H			
	N3$\cdots$H–O$\cdots$H–NH		
ΔE	−31.80	−42.92	−40.98
$\Delta E + \Delta ZPE$	−24.18	−35.30	−32.19
$\Delta E + \Delta ZPE - BSSE$	−21.54	−27.33	−28.71
	N7H$\cdots$OH$_2$		
ΔE	−29.02	−38.07	−31.48
$\Delta E + \Delta ZPE$	−23.18	−32.22	−25.65
$\Delta E + \Delta ZPE - BSSE$	−20.04	−24.18	−21.59
	N1$\cdots$H–O$\cdots$H–NH		
ΔE	−26.44	−37.07	−36.46
$\Delta E + \Delta ZPE$	−18.72	−29.35	−27.75
$\Delta E + \Delta ZPE - BSSE$	−16.24	−21.89	−24.56
	N9$\cdots$H–OH		
ΔE	−27.14	−34.20	−31.26
$\Delta E + \Delta ZPE$	−20.82	−27.88	−24.31
$\Delta E + \Delta ZPE - BSSE$	−18.75	−22.18	−21.80

and −322 cm^{-1} for these complexes, respectively. The weak shoulder at 3 310 cm^{-1} might be responsible for the $\nu^{\mathrm{b}}_{\mathrm{O\text{-}H}}$ of the third complex, N3$\cdots$H–O$\cdots$H–NH (indicated with a dotted arrow in Fig. 4).

An additional argument for the rather tentative assignments of the $\nu^{\mathrm{b}}_{\mathrm{O\text{-}H}}$ modes of the complexes (1), (2) and (4) is obtained by additional experiments in a D_2O-doped Ar matrix. Figure 5 illustrates the region between 2 800 and 2 400 cm^{-1} of the spectrum of 2AP/D_2O/Ar. All the D_2O and DOH bands in this spectrum agree well with the assignments published by Engdahl *et al.* [31]. However, three additional bands appear at 2 590, 2 563 and 2 516 cm^{-1}. Using the earlier assigned $\nu^{\mathrm{b}}_{\mathrm{O\text{-}H}}$ modes at 3 407, 3 392 and 3 301 cm^{-1}, the isotopic ratios $\nu^{\mathrm{b}}_{\mathrm{O\text{-}H}}/\nu^{\mathrm{b}}_{\mathrm{O\text{-}D}}$ can be calculated. The obtained values are 1.315, 1.323 and 1.312. For H-bonded complexes of this strength, these values are quite acceptable [32]. We should mention that some of the complex bands, *e.g.* 3 700 cm^{-1}, 3 392 cm^{-1}, have frequencies close to either $(H_2O)_n$ or $(H_2O)_3$ bands, respectively and one may doubt about their assignments as complex bands. However, the possibility that the alternative assignment would be the correct one is ruled out by the observation that the bands do not occur in matrix spectra of water complexes, with other bases, *e.g.* 6-mercaptopurine [29].

The frequency shifts of the $\nu^{\mathrm{a}}_{\mathrm{NH_2}}$ and $\nu^{\mathrm{s}}_{\mathrm{NH_2}}$ modes of the N3$\cdots$H–O$\cdots$H–N9 complex are negligibly small. Shifts of these vibrational modes are only significant in complexes

Table 3. Experimental (Ar matrix) and calculated (DFT/B3LYP/6-31++G**) IR spectral data (3 800–3 100 cm^{-1}) for the four H-bonded complexes of the amino–N9H form of 2-aminopurine with water.

Experimental		Calculated (DFT/B3LYP)				PED[d]
ν (cm^{-1})	$\Delta\nu$ (cm^{-1})[a]	ν(cm^{-1}) scaled[b]	I(km mol^{-1})	$\Delta\nu$(cm^{-1})[a]	optimal scaling factor[c]	
			N3$\cdots$H–O$\cdots$H–N9			
3 700	−34	3 696	95	−39	0.951	ν^f(OH)(99)
3 392 → 3 406[e]	−246 → −280[e]	3 385	752	−233	0.952	ν^b(OH)(78) + ν(N9H)(20)
[f]		3 553	48	−8		ν^a(NH$_2$) (100)
[f]		3 429	75	−4		ν^s(NH$_2$) (100)
3 363 ?	−132	3 348	38	−131	0.954	ν(N9H) (80) + ν^b(OH) (19)
			N1$\cdots$H–O$\cdots$H–NH			
3 700	−34	3 692	80	−43	0.952	ν^f(OH) (100)
3 301 → 3 315[e]	−337 → −371[e]	3 296	430	−322	0.951	ν^b(OH) (85) + ν^s(NH$_2$) (10)
3 544	−20	3 541	111	−20	0.951	ν^a(NH$_2$) (86) + ν^s(NH$_2$) (15)
3 368	−81	3 358	751	−75	0.953	ν^s(NH$_2$) (75) + ν^a(NH$_2$) (12) + ν^b(OH) (13)
			N3$\cdots$H–O$\cdots$H–NH			
3 700	−34	3 690	91	−44	0.953	ν^f(OH) (100)
3 310? → 3 324[e]	−328 → −362[e]	3 336	130	−292	0.942	ν^b(OH) (62) + ν^s(NH$_2$) (30)
3 544	−20	3 544	123	−17	0.950	ν^a(NH$_2$) (88) + ν^s(NH$_2$) (13)
3 384	−65	3 375	790	−58	0.952	ν^s(NH$_2$) (57) + ν^a(NH$_2$) (34)
			N7$\cdots$H–OH			
3 700	−34	3 693	96	−42	0.952	ν^f(OH) (98)
3 407 → 3 421[e]	−231 → −265[e]	3 414	837	−204	0.950	ν^b(OH) (94)

[a] Shift with respect to experimental or calculated monomer frequencies. [b] Scaling factor: 0.950.
[c] Optimal scaling factor = $\nu_{exp}/\nu_{calc(unscaled)}$.
[d] ν = stretching, f = free, non hydrogen-bonded, b = hydrogen-bonded, a = asymmetric, s = symmetric.
[e] ν(OH) is corrected for reduced coupling in bonded water. [f] Not possible to distinguish from the monomer bands.

Table 4. Experimental (Ar matrix) and calculated (DFT/B3LYP/6-31++G**) IR spectral data (1 700–1 400 cm^{-1}) for the four H-bonded complexes of the amino–N9H form of 2-aminopurine with water.

Experimental		Calculated (DFT/B3LYP)				PED[d]
ν (cm^{-1})	$\Delta\nu$ (cm^{-1})[a]	ν(cm^{-1}) scaled[b]	I(km mol^{-1})	$\Delta\nu$(cm^{-1})[a]	optimal scaling factor[c]	
			N3$\cdots$H–OH$\cdots$H–N9			
1 624	+33	1 592	31	+32	0.994	δ(H$_2$O) (74) + δ(N9H) (20)
1 608	+18	1 574	162	+14	0.996	δ(H$_2$O) (28) + ν(C5C6)(21) + ν(C4C5)(15)
1 598	+3	1 601	282	+4	0.973	δ(NH$_2$) (64) + δ(H$_2$O) (14) + ν(C2N) (10)
1 417	+37	1 384	45	+15	0.999	δ(N9H) (39) + ν(C8N9) (17)
			N1$\cdots$H–O$\cdots$H–NH			
1 624	+33	1 588	88	+28	0.997	δ(H$_2$O) (87)
1 624	+29	1 624	160	+27	0.975	δ(NH$_2$) (69) + δ(H$_2$O) (17)
			N3$\cdots$H–O$\cdots$H–NH			
1 624	+33	1 582	66	+22	1.000	δ(H$_2$O) (100)
1 624	+29	1 620	179	+23	0.977	δ(NH$_2$) (70) + δ(H$_2$O) (14) + ν(C2N) (11)
			N7$\cdots$H–OH			
1 624	+33	1 595	30	+35	0.993	δ(H$_2$O) (89)

[a] Shift with respect to experimental or calculated monomer frequencies. [b] Scaling factor: 0.975.
[c] Optimal scaling factor = $\nu_{exp}/\nu_{calc\ (unscaled)}$. [d] ν = stretching, δ = bending.

Table 5. Experimental (Ar matrix) and calculated (DFT/B3LYP/6-31++G**) IR spectral data (800–400 cm^{-1}) for the four H-bonded complexes of the amino–N9H form of 2-aminopurine with water.

Experimental		Calculated (DFT/B3LYP)				PED[d]
ν (cm^{-1})	$\Delta\nu$ (cm^{-1})[a]	ν(cm^{-1}) scaled[b]	I(km mol^{-1})	$\Delta\nu$(cm^{-1})[a]	optimal scaling factor[c]	
			N3···H–O···H–N9			
670	/	670	132	/	0.980	τ^1(···OHH···) (60) + τ^2(···OHH) (26)[e]
410	/	409	104	/	0.983	τ^1(···OHH···) (32) + τ^2(···OHH) (36)[e]
690	+187	714	86	+214	0.999	γ(N9H) (38) + $\tau r1$(22) + γ(C2N) (14)
487	0	460	65	0	1.038	τ(NH_2) (48) + wag(NH_2) (14) + $\delta R3$ (12)
[f]		392	255	+41		wag(NH_2) (69) + τ(NH_2) (12)
			N1···H–O···H–NH			
?	/	749	171	/	0.982	τ^1(···OHH···) (97)[e]
410	/	412	138	/	0.974	τ^2(···OHH···) (61)[f] + δ(···OHH···)(14) + τ(NH_2) (12) + $\tau R2$ (11)
630	+143	622	62	+162	0.992	τ(NH_2) (56)
[f]		316	138	−35		wag(NH_2) (44) + $\tau r1$ (11) + τrR (12)
			N3···H–O···H–NH			
?		742	158	/	0.991	τ^1(···OHH···) (61) + τ^2(···OHH···)(22) + δ(···OHH···) (12)[e]
410		400	152	/	1.005	τ^2(···OHH···) (41) + τ^1(···OHH···)(23) + wag(NH_2) (15) + τ(NH_2) (11)[e]
630	+143	631	37	+171	0.978	τ(NH_2) (34) + $\delta r2$ (14) + γ(C2N) (10)
[f]		319	89	−31		wag(NH_2) (34) + τ^2(···OHH···) (32)
			N7···H–OH			
670		662	94	/	0.987	δ(N···H–O) (69) + wag oop (N···H–O) (26)[e]
[f]		365	105	/		wag(N···H–O) (70) + δ(N···H–O) (20)[e]

[a]Shift with respect to experimental or calculated monomer frequencies. [b]Scaling factor: 0.98.
[c] Optimal scaling factor = $\nu_{exp}/\nu_{calc\ (unscaled)}$. [d]$\delta$ = bending, τ = torsion, γ = out of plane motion, wag = wagging.
[e] τ^1 and τ^2 = new intermolecular torsion modes. [f] Situated below the studied region.

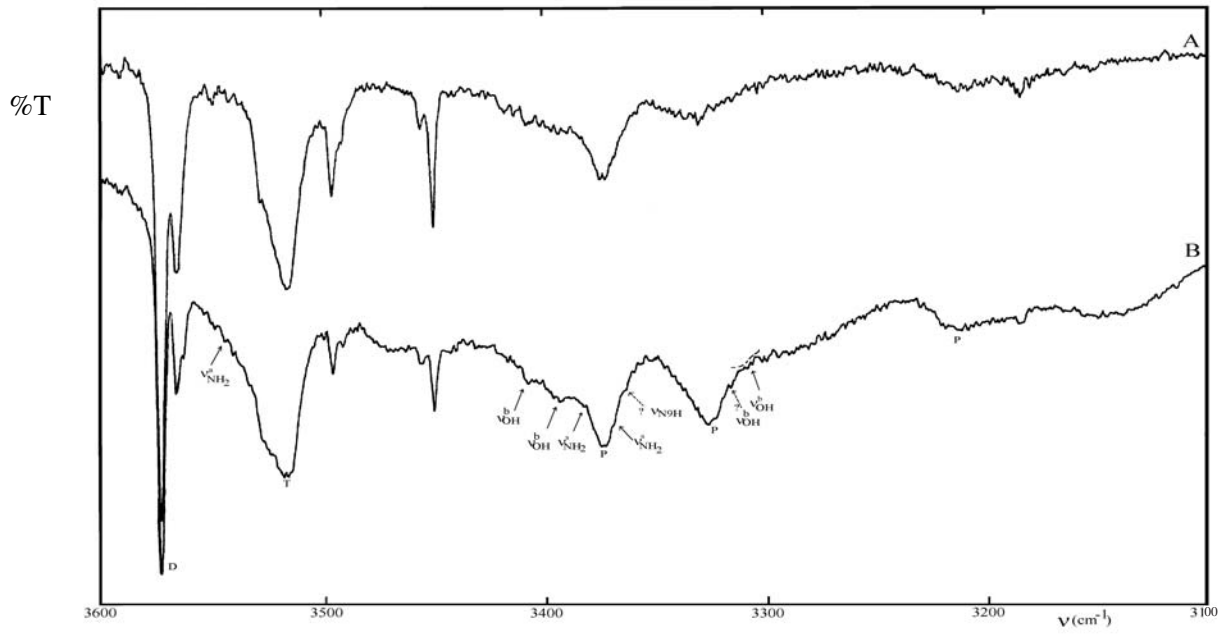

Fig. 4. The 3 600–3 100 cm^{-1} region of the FT-IR spectrum of 2-aminopurine/H_2O/Ar (H_2O/Ar: 1/250) (A) before annealing and (B) after annealing.

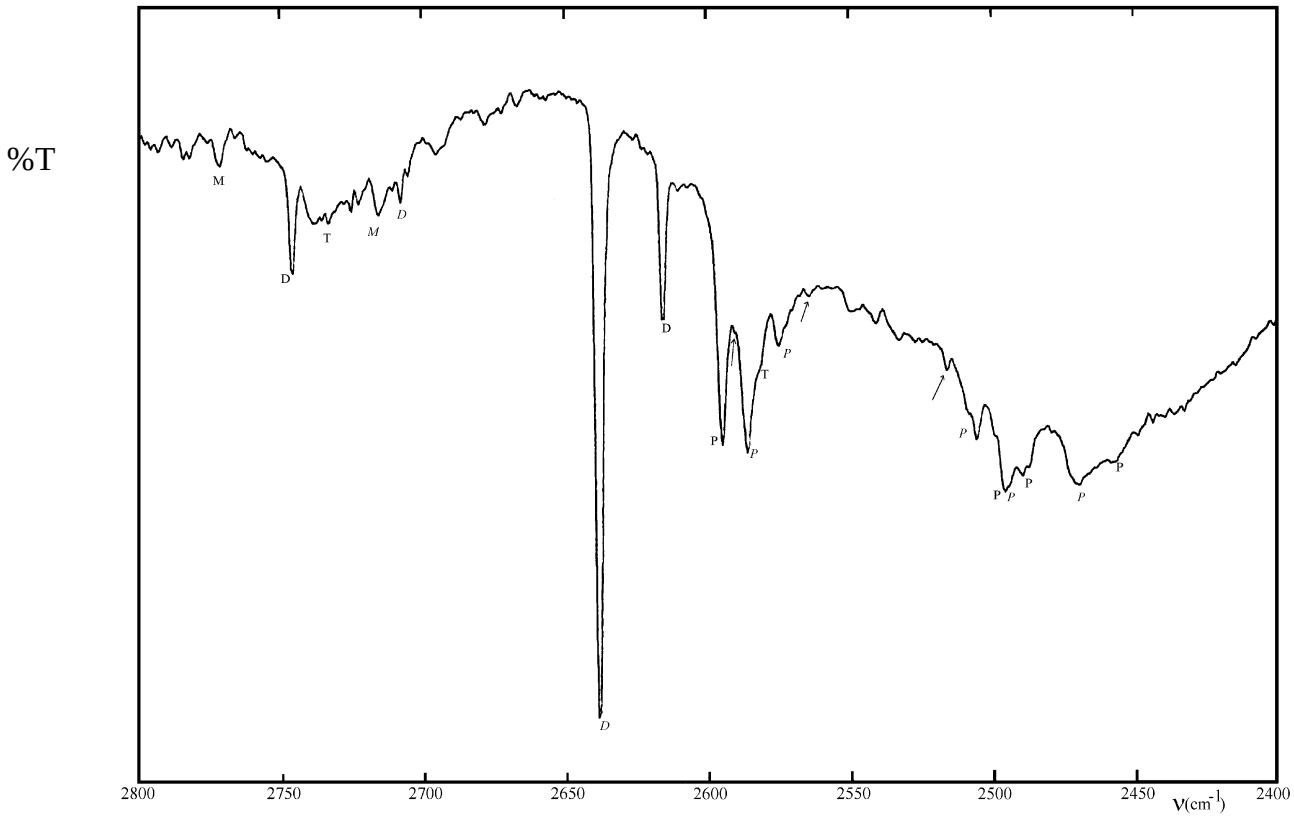

Fig. 5. The 2 800–2 400 cm^{-1} region of the FT-IR spectrum of 2-aminopurine/D_2O/Ar (D_2O/Ar: 1/100).

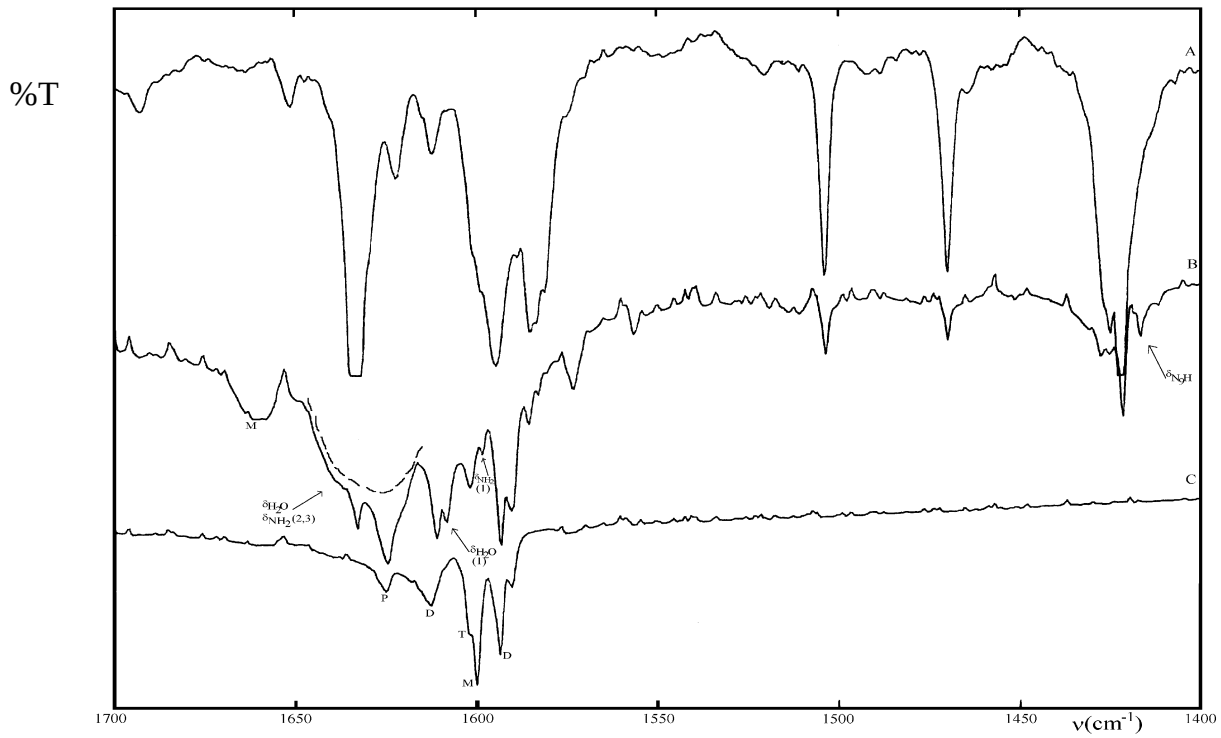

Fig. 6. The 1 700–1 400 cm^{-1} region of the FT-IR spectrum of 2-aminopurine/Ar (A), 2-aminopurine/H_2O/Ar (H_2O/Ar: 1/250) (B) and H_2O/Ar (H_2O/Ar: 1/300) (C).

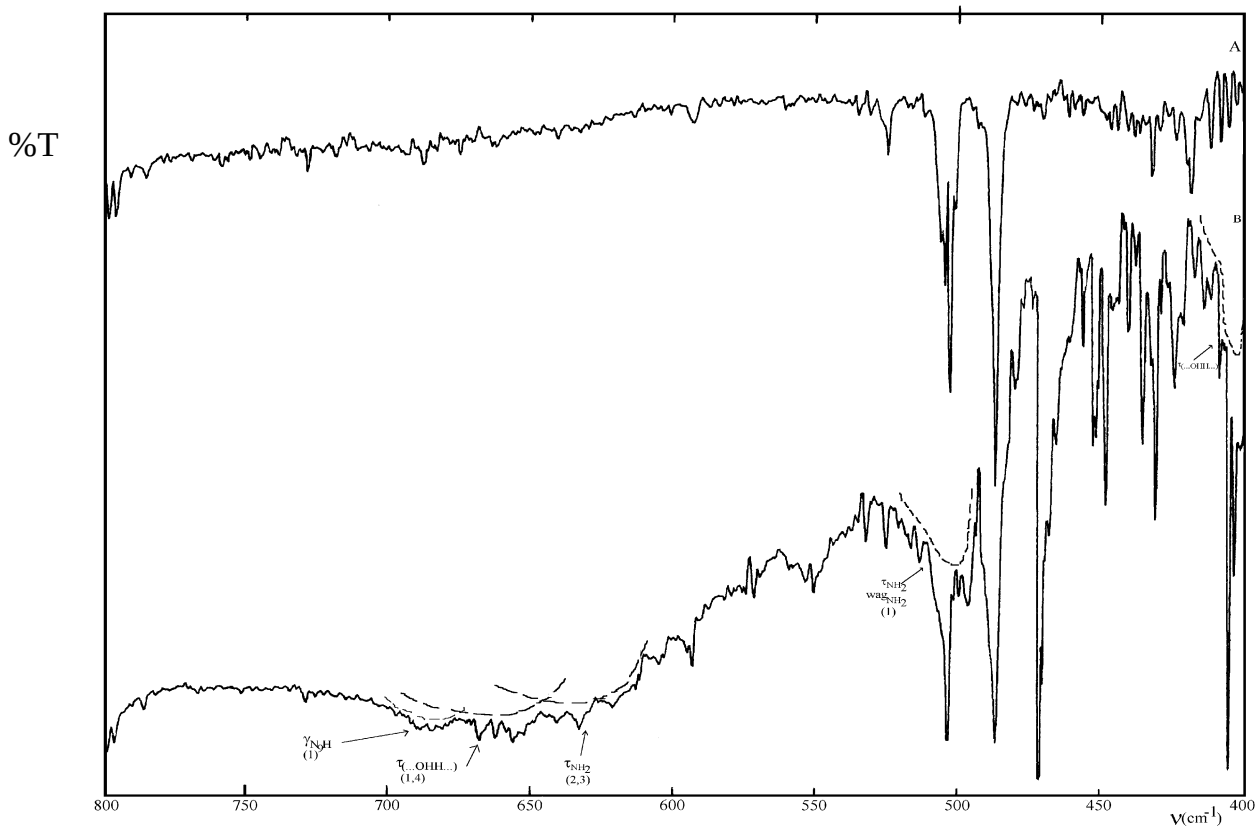

Fig. 7. The 800–400 cm^{-1} region of the FT-IR spectrum of 2-aminopurine/H_2O/Ar (H_2O/Ar: 1/800) before annealing (A) and 2-aminopurine/H_2O/Ar (H_2O/Ar: 1/250) after annealing (B).

in which the NH_2-group is involved in the H-bond, *i.e.* N1···H–O···H–NH and N3···H–O···H–NH. The intensities of these bands are also much larger in the latter type of complexes.

The high-frequency shoulder on the absorption of trimer water at about 3 544 cm^{-1} (Fig. 4) is possibly due to the $\nu^{a}_{NH_2}$ of the two N···H–O···H–NH complexes, the shift of -20 cm^{-1} being comparable to the predicted shifts of -20 and -17 cm^{-1}, respectively.

The symmetric stretching $\nu^{s}_{NH_2}$ bands are more intense. The $\nu^{s}_{NH_2}$ mode of the N1···H–O···H–NH and N3···H–O···H–NH are predicted to shift -75 and -58 cm^{-1}, respectively. This implies that these new bands are situated in the same region as the bonded O–H stretching vibrations of water. Some weak shoulders within the broad band at 3 400–3 370 cm^{-1} must be responsible for the symmetric stretching vibration of the NH_2 group of the two N···H–O···H–NH complexes, probably at 3 368 and 3 384 cm^{-1}.

The $\nu_{N9\text{-}H}$ frequency of the N3···H–O···H–N9 complex has a predicted frequency shift of -131 cm^{-1}. From the experimental monomer absorption of 3 495 cm^{-1}, this complex band is expected to be located at about 3 364 cm^{-1}. Because its predicted intensity is very small (38 km mol^{-1}), the identification of this band is difficult. The weak shoulder at 3 363 cm^{-1} can tentatively be assigned to this band.

3.2.3 δ_{H_2O} and $\delta_{N\text{-}H}$ region

Figure 6 illustrates the OH and NH bending vibration region of the monomer 2AP/Ar spectrum (A), the complex spectrum (B) and the spectrum of pure water/Ar (C). Complex formation is clearly manifested in spectrum B by considerable intensity differences compared to spectrum C.

The predicted shifts for the δ_{H_2O} modes vary from +22 to +35 cm^{-1} for the four complexes. The similar shifts and the large intensity of the monomer, dimer, trimer δ_{H_2O} bands makes it difficult to detect the different complexes separately. The band at 1 624 cm^{-1} in spectrum B is much broader and larger than the band at 1 624 cm^{-1} in spectrum C, which originates from polymer δ_{H_2O} absorptions in pure water/Ar. This intense absorption band in spectrum B must therefore be due to a combination of the different δ_{H_2O} bending modes of all four complexes, overlapping with the polymer water absorptions. The δ_{NH_2} vibrations of the two N···H–O···H–NH complexes (indicated by 2 and 3 in Fig. 6) are also situated in this region. The new band at 1 608 cm^{-1} in the complex spectrum is due to the combination band (δ_{H_2O} + ν_{C5C6} +ν_{C4C5}) of the N3···H–O···H–N9 complex (Tab. 4). This band is predicted with a large intensity at 1 574 cm^{-1}. From this prediction, the experimental absorption must be situated around 1 605 cm^{-1}, which agrees well with the assignment at 1 608 cm^{-1}.

The δ_{NH_2} mode of the N3···H–O···H–N9 complex is shifted only +4 cm^{-1} theoretically, the intensity being predicted to be rather high. Although the frequency difference with the monomer absorption suggests that the complex band is difficult to identify, a new band at 1 598 cm^{-1} appears in spectrum B. This band is tentatively assigned to the δ_{NH_2} band of this first complex.

The δ_{N9H} vibration of the bonded N9–H group in the N3···H–O···H–N9 complex is expected to shift +15 cm^{-1} with respect to the monomer N9–H bending vibration. The new band at 1 417 cm^{-1} in the complex spectrum is most probably responsible for this vibration.

3.2.4 $\tau(\cdots H_2O\cdots)$, γ(N–H), $\tau(NH_2)$ and wag(NH_2) region

Some new intermolecular τ modes of H-bonded water are predicted in the low-frequency spectral region (Tab. 5). Usually these bands appear as rather broad bands in the experimental spectrum. The theoretical predictions of the new, intermolecular torsion vibrations of water are 670, 749, 742 and 662 cm^{-1} for the four complexes, in decreasing order of stability. Figure 7 illustrates the low frequency region of the complex spectra of 2AP with water.

A first new, broad band appears at about 670 cm^{-1}. The assignment of this band to the intermolecular torsion vibration of the N3···H–O···H–N9 complex and, to less extent, to the N7···H–OH complex seems reasonable. The identification of the intermolecular torsion bands of the two N···H–O···H–NH complexes is more difficult.

Another combination of the new intermolecular torsion vibrations is predicted around 400 cm^{-1} for all four complexes. In the experimental spectrum an intense, broad band is indeed identified at 410 cm^{-1}.

The out-of-plane vibration of the N9–H group in the N3···H–O···H–N9 is shifted theoretically by not less than +214 cm^{-1}. The band at 690 cm^{-1} might be due to the out-of-plane of this bonded N–H group. The experimental shift of +187 cm^{-1} agrees well with the theoretically predicted value.

The amino group of the N3···H–O···H–N9 complex is not involved in the H-bond, which explains why the theoretical shift of τ_{NH_2} in combination with wag (NH_2) is 0 cm^{-1}. Nevertheless, the position of the NH_2 group near the H-bond causes this band to become much broader, the center of the band being still located at 487 cm^{-1}.

The broad band at about 630 cm^{-1}, partly overlapping with the band at 670 cm^{-1}, is due to the torsion mode of the NH_2 groups of the two N···H–O···H–NH complexes. These bands are theoretically predicted at 622 and 631 cm^{-1} for the N1···H–O···H–NH and the N3···H–O···H–NH complexes, respectively.

Although some assignments for each complex are without doubt tentative, the vibrational analysis of the experimental complex spectra of 2-aminopurine·H_2O clearly confirms the presence of the four complexes of the amino N9H tautomer, as was predicted by the theoretical calculations.

The optimal scaling factors, calculated as ν_{exp}/ν_{calc}, agree well with the optimal scaling factors usually found in similar H-bond complexes [22,33] as well as with the scaling factors normally applied in the scaling procedure with variable scaling factors [19,34]. Especially the $\nu_{X\text{-}H}$ mode scaling factor of 0.950 corresponds well.

For some absorption bands for which the assignments are not very accurate because of overlap of different vibrations, *e.g.* δ_{H_2O} and the δ_{NH_2}, the scaling factor values are not as satisfying as for the well-separated bands.

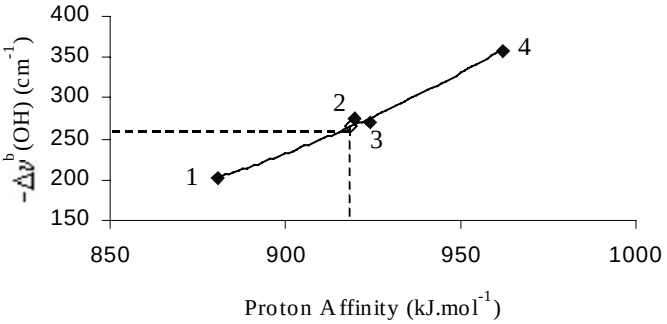

Fig. 8. Correlation between the corrected frequency shift $\Delta\nu^{b}_{OH}$ (cm^{-1}) and the proton affinity ($kJ\,mol^{-1}$) of the basic N atom in open N···H–OH complexes.

4 Correlation

The experimental-theoretical approach applied in this work can be used to demonstrate some interesting and useful correlations between theoretical and experimental H-bond parameters.

A first correlation to be examined is the correlation between the frequency shift $\Delta\nu^{b}_{OH}$ of the bonded OH group and the proton affinity of the proton acceptor N atom in open N···H–OH complexes.

From an earlier study on H-bonded complexes of water with different cytosine model compounds (pyrimidine, pyridine, imidazole and 4-aminopyridine), a 4-point correlation between the experimental $\Delta\nu^{b}_{OH}$ values in N···H–OH complexes and the proton affinity values of the N atom in these molecules was obtained [35]. This correlation has been used to estimate unknown PA values of particular N atoms in polyfunctional bases such as cytosines, adenines and guanines. Figure 8 illustrates this mentioned 4-point correlation.

Only one open N···H–OH complex has been identified experimentally in this work, *i.e.* the N7···H–OH complex. The experimental frequency shift $\Delta\nu^{b}_{OH}$ for this open complex can be used to estimate the (until now "unknown") proton affinity value of the N7 atom in 2AP.

From the experimental frequency shift of the bonded O–H vibration in the N7···H–OH complex of 2AP with water, the PA value of the N7 atom can be estimated as 919 $kJ\,mol^{-1}$. This value is close to the PA value of the N7 atom in non-substituted purine (917.5 $kJ\,mol^{-1}$) [36]. The fact that the PA values of the N7 atom in purine and in 2–NH_2–purine are so close can be explained by considering the resonance forms of 2–NH_2–purine. No resonance structure with $N7^{\ominus}$ can be obtained in 2–NH_2–purine which

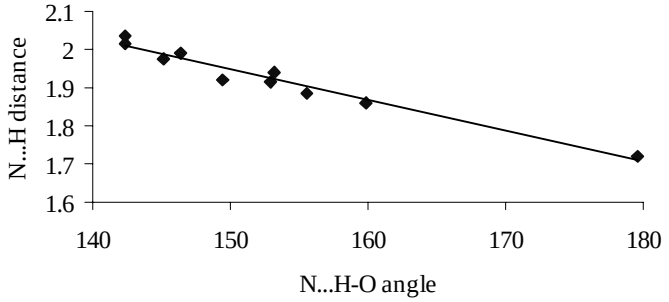

Fig. 9. Correlation between the N···H H-bond distance (Å) and the N···H–O angle (°) for closed H-bonded complexes N···H–O···H–N.

therefore suggests a N7 basicity similar to that of N7 in purine.

A more recent developed correlation is that between H-bond linearity and H-bond cooperativity [37].

This mutual relation between the H-bond non-linearity and the cooperativity is illustrated in Figure 9 where the N···H H-bond distance is plotted *versus* the angle N···H–O in closed N···H–O···H–N complexes. The smallest H-bond distance or strongest H-bond is found in the symmetric, closed homo-dimer of 2-pyridone [38] where both H-bonds in the complex are almost linear (180°) and the optimal cooperativity effect is reflected by a very large interaction energy (−83.8 kJ mol). For the other complexes in this correlation, *i.e.* N···H–O···H–N complexes of 2-aminopurine, hypoxanthine, 6-mercaptopurine, adenine and 4-aminobenzimidazole, the cooperativity effect is reduced because of the deviation of the N···H–O angle from 180°. Therefore, a clear dependence of H-bond strength from H-bond non-linearity is demonstrated for the first time for a larger series of comparable complexes.

5 Conclusions

The combined matrix-isolation FT-IR and theoretical RHF, MP2 and DFT(B3LYP)/6-31++G** method has been applied to investigate the tautomeric and H-bonding characteristics of 2-aminopurine. The theoretical assisted analysis of the experimental FT-IR spectrum of 2-aminopurine in Ar demonstrates the overwhelming presence of the amino–N9H tautomer and to a less extent the amino–N7H tautomer. Combination of experimental and theoretical predicted IR intensities of some characteristic bands of both tautomers allows to estimate a tautomerization constant K_T (amino–N7H/amino–N9H) of 0.016 at the RHF level and 0.015 at the DFT level of theory. Four stable H-bonding complexes with water exist for the amino–N9H tautomer. The amino–N7H tautomer can also form four H-bonding complexes with water. The four complexes of the amino–N9H form, *i.e.* N3···H–O···H–N9, N1···H–O···H–NH, N3···H–O···H–NH and N7···H–OH, are more stable than the complexes of the amino–N7H and all were identified in the experimental spectrum. The three closed complexes are more stable than the open complex, because of the cooperativity effect. The experimental frequency shift of the bonded O–H vibration in the open N7···H–OH complex was used in an earlier established correlation to estimate the proton affinity of the N7 atom in 2-aminopurine. A second correlation between the N···H H-bond distance *versus* the angle N···H–O in closed N···H–O···H–N H-bond complexes shows a clear dependence of the H-bond strength from the linearity of the H-bond.

R. Ramaekers acknowledges financial support from the Flemish Institute for the Promotion of the Scientific-Technological Research in Industry (IWT).

References

1. P.A. Fagan, C. Fàbrega, R. Eritja, M.F. Goodman, D.E. Wemmer, Biochemistry **35**, 4026 (1996)
2. L.C. Sowers, Y. Boulard, G.V. Fazakerley, Biochemistry **39**, 7613 (2000)
3. G.G. Sheina, S.G. Stepanian, E.D. Radchenko, Yu.P. Blagoi, J. Mol. Struct. **158**, 275 (1987)
4. A. Broo, A. Holmén, Chem. Phys. **211**, 147 (1996)
5. A. Holmén, J. Phys. Chem. A **101**, 4361 (1997)
6. S.K. Mishra, M.K. Shukla, P.C. Mishra, Spectrochim. Acta A **56**, 1355 (2000)
7. J.M. Jean, K.B. Hall, J. Phys. Chem. A **104**, 1930 (2000)
8. E.L. Rachofsky, J.B.A. Ross, M. Krauss, R. Osman, J. Phys. Chem. A **105**, 190 (2001)
9. E. Nir, K. Kleinermanns, L. Grace, M.S. de Vries, J. Phys. Chem. A **105**, 5106 (2001)
10. P.A. Fagan, C. Fàbrega, R. Eritja, M.F. Goodman, D.E. Wemmer, Biochemistry **35**, 4026 (1996)
11. L.C. Sowers, Y. Boulard, G.V. Fazakerley, Biochemistry **39**, 7613 (2000)
12. E.C. Sherer, C.J. Cramer, J. Comp. Chem. **22**, 1167 (2001)
13. G. Maes, Bull. Soc. Chim. Belg. **90**, 1093 (1981)
14. A. Destexhe, J. Smets, L. Adamowicz, G. Maes, J. Phys. Chem. **98**, 1506 (1994)
15. M. Graindourze, J. Smets, Th. Zeegers-Huyskens, G. Maes, J. Mol. Struct. **222**, 345 (1990)
16. P.J. Stephens, F.J. Devlin, C.F. Chabalowski, M.J. Frisch, J. Phys. Chem. **98** 11623 (1994)
17. C. Lee, W. Yang, R.G. Parr, Phys. Rev. B **37**, 785 (1998)
18. M.K. van Bael, K. Schoone, L. Houben, J. Smets, W. McCarthy, L. Adamowicz, M.J. Nowak, G. Maes, J. Phys. Chem. A **101**, 2397 (1997)
19. K. Schoone, J. Smets, L. Houben, M.K. van Bael, L. Adamowicz, G. Maes, J. Phys. Chem. A **102**, 4863 (1998)
20. J. Smets, K. Schoone, R. Ramaekers, L. Adamowicz, G. Maes, J. Mol. Struct. **442**, 201 (1998)
21. R. Ramaekers, G. Maes, L. Adamowicz, A. Dkhissi, J. Mol. Struct. **560**, 205 (2001)
22. R. Ramaekers, W. Dehaen, L. Adamowicz, G. Maes, J. Phys. Chem. (in press)
23. S.F. Boys, F. Bernardi, Mol. Phys. **19**, 553 (1970)
24. J. Florian, B.G. Johnson, J. Phys. Chem. **98**, 3681 (1994)
25. G. Rauhut, P. Pulay, J. Phys. Chem. **99**, 3093 (1995)
26. J. Florian, J. Leszczynski, J. Phys. Chem. **100**, 5578 (1996)

27. *Gaussian94*, Revision E.2, M.J. Frisch, G.W. Trucks, H.B. Schlegel, P.M.W. Gill, B.G. Johnson, M.A. Robb, J.R. Cheeseman, T. Keith, G.A. Petersson, J.A. Montgomery, K. Raghavachari, M.A. Al-Laham, V.G. Zakrzewski, J.V. Ortiz, J.B. Foresman, J. Cioslowski, B.B. Stefanov, A. Nanayakkara, M. Challacombe, C.Y. Peng, P.Y. Ayala, W. Chen, M.W. Wong, J.L. Andres, E.S. Replogle, R. Gomperts, R.L. Martin, D.J. Fox, J.S. Binkley, D.J. Defrees, J. Baker, J.P. Stewart, M. Head-Gordon, C. Gonzales, J.A. Pople, Gaussian Inc., Pittsburgh, PA, 1995
28. *Gaussian98*, Revision A.5, M.J. Frisch, G.W. Trucks, H.B. Schlegel, G.E. Scuseria, M.A. Robb, J.R. Cheeseman, V.G. Zakrzewski, J.A. Montgomery, R.E. Stratmann, J.R. Burant, S. Dapprich, J.M. Millam, A.D. Daniels, K.N. Kudin, M.C. Strain, O. Farkas, J. Tomasi, V. Barone, M. Cossi, R. Cammi, B. Mennucci, C. Pomelli, C. Adamo, S. Clifford, J. Ochterski, G.A. Petersson, P.Y. Ayala, Q. Cui, K. Morokuma, D.K. Malick, A.D. Rabuck, K. Raghavachari, J.B. Foresman, J. Cioslowski, J.V. Ortiz, B.B. Stefanov, G. Liu, A. Liashenko, P. Piskorz, I. Komaromi, R. Gomperts, R.L. Martin, D.J. Fox, T. Keith, M.A. Al-Laham, C.Y. Peng, A. Nanayakkara, C. Gonzalez, M. Challacombe, P.M.W. Gill, B.G. Johnson, W. Chen, M.W. Wong, J.L. Andres, M. Head-Gordon, E.S. Replogle, J.A. Pople, Gaussian Inc., Pittsburgh, PA, 1998
29. R. Ramaekers, Ph.D. thesis, KU Leuven, 2001
30. G. Maes, J. Smets, J. Phys. Chem. **97**, 1818 (1993)
31. A. Engdahl, B. Nelander, J. Mol. Struct. **193**, 101 (1989)
32. J. Smets, Ph.D. thesis, KU Leuven, 1993
33. R. Ramaekers, A. Dkhissi, L. Adamowicz, G. Maes, J. Phys. Chem. A **106**, 4502 (2002)
34. A. Dkhissi, L. Adamowicz, G. Maes, J. Phys. Chem. A **104**, 2112 (2000)
35. J. Smets, L. Adamowicz, G. Maes, J. Phys. Chem. **99**, 6387 (1995)
36. S.G. Lias, J.F. Liebman, R.D. Levin, J. Phys. Chem. **13**, 695 (1984)
37. L. Houben, Ph.D. thesis, KU Leuven, 2000
38. A. Dkhissi, R. Ramaekers, L. Houben, L. Adamowicz, G. Maes, Chem. Phys. Lett. **331**, 553 (2000)